CORA Cork Open Research Archive
Cartlann Taighde Oscailte Chorcaí

Title	Kinematic analysis of a single-loop reconfigurable 7R mechanism with multiple operation modes
Authors	He, Xiuyun;Kong, Xianwen;Chablat, Damien;Caro, Stéphane;Hao, Guangbo
Publication date	2014
Original Citation	Xiuyun He, Xianwen Kong, Damien Chablat, Stéphane Caro and Guangbo Hao. (2014) Kinematic analysis of a single-loop reconfigurable 7R mechanism with multiple operation modes . Robotica, available on CJO2014. doi:10.1017/S0263574713001197.
Type of publication	Article (peer-reviewed)
Link to publisher's version	http://journals.cambridge.org/action/displayJournal?jid=ROB - 10.1017/S0263574713001197
Rights	Copyright © Cambridge University Press 2014. This article has been accepted for publication and will appear in a revised form, subsequent to peer review and/or editorial input by Cambridge University Press, in Robotica published by Cambridge University Press http://dx.doi.org/10.1017/S0263574713001197
Download date	2026-11-06 23:12:19
Item downloaded from	https://hdl.handle.net/10468/1525

UCC
University College Cork, Ireland
Coláiste na hOllscoile Corcaigh

Kinematic analysis of a single-loop reconfigurable 7R mechanism with multiple operation modes

Xiuyun He†, Xianwen Kong†,1, Damien Chablat‡, Stéphane Caro‡, Guangbo Hao§

†*School of Engineering and Physical Sciences, Heriot-Watt University, Edinburgh, EH14 4AS, UK*

‡*Institut de Recherche en Communications et en Cybernétique de Nantes (IRCCyN), Université Nantes Angers Le Mans, Nantes, France*

§*School of Engineering, University College Cork, Cork, Ireland*

ABSTRACT

This paper presents a novel 1-DOF (degree-of-freedom) single-loop reconfigurable 7R mechanism with multiple operation modes (SLR7RMMOM), composed of seven revolute (R) joints, via adding a revolute joint to the overconstrained Sarrus linkage. The SLR7RMMOM can switch from one operation mode to another without disconnection and reassembly, and is a non-overconstrained mechanism. The algorithm for the inverse kinematics of the serial 6R mechanism using kinematic mapping is adopted to deal with the kinematic analysis of the SLR7RMMOM. Firstly, a numerical method is applied and an example is given to show that there are 13 sets of solutions for the SLR7RMMOM corresponding to each input angle. Among these solutions, nine sets are real solutions, which are verified using both the CAD model and the prototype of the mechanism. Then an algebraic approach is also used to analyze the mechanism and the same results are obtained as the numerical one. It is shown from both the numerical and algebraic approaches that the SLR7RMMOM has three operation modes: translational mode and two 1-DOF planar modes. The transitional configurations among the three modes are also identified.

KEYWORDS: *Single-loop reconfigurable mechanism; Multiple operation modes; Kinematic analysis; Numerical method; Algebraic approach; Transitional configuration*

1. Introduction

Reconfigurable mechanisms (RMs) have received increasing attention from researchers around the world, which can generate different operation modes to fulfil variable tasks based on a sole mechanism. Different approaches have been proposed to design RMs generating multiple motion patterns. Several classes of RPMs have been developed such as modular reconfigurable mechanisms[1,2], metamorphic mechanisms[3], kinematotropic mechanisms[4], variable actuated mechanisms[5], and reconfigurable mechanisms with multiple operation modes[6-8].

This paper focuses on the reconfigurable mechanism with multiple operation modes[6-9] since this class of RMs can be reconfigured without disassembly and without increasing the number of actuators. One design approach has been proposed in [6-8] for the synthesis of reconfigurable mechanisms with multiple operation modes, including single-loop reconfigurable mechanisms with multiple operation modes[6,7] and multiple-loop reconfigurable mechanisms with multiple operation modes[8]. An intuitive approach[6] was proposed to construct a single-loop reconfigurable mechanism with multiple operation modes by combining two overconstrained mechanisms. Using this approach, Huang et al[7] proposed a spatial 7-link mechanism by combining a Bennett linkage and a RPRP linkage (R: revolute joint; P: prismatic joint) and revealed that the mechanism has three operation modes: the 5R2P, Betnett and RPRP modes. Another design approach for constructing single-loop reconfigurable mechanisms with multiple operation modes is to insert one or more joints into an overconstrained mechanism[17]. In this paper, we will propose a new 7R mechanism by inserting one R joint into the overconstrained Sarrus linkage. This mechanism has at least two operation modes: the Sarrus linkage motion mode (translational mode) and one planar mode. One apparent merit of the new 7R mechanism, compared to the original Sarrus linkage or other conventional single-mode 7R mechanisms is that it has multiple operation modes.

Meanwhile, several analysis approaches have been developed to deal with the kinematics and singularity analysis of serial and parallel mechanisms, such as differential algorithm[10], screw theory algorithm[11] and kinematic mapping algorithm[13]. Husty and Pfurner have made a significant contribution to the kinematic mapping algorithm to the kinematic analysis of mechanisms[12-16]. It has been shown that kinematic mapping algorithm is very efficient for both direct (forward) and inverse kinematic analysis of mechanisms.

The kinematic analysis of the single-loop reconfigurable 7R mechanism with multiple operation modes (SLR7RMMOM) proposed in this paper is to be analyzed using the effective algorithm for the inverse kinematics of a general serial 6R manipulator. The operational modes and transitional configurations will be identified. The paper is organised as follows. Section 2 describes the 1-DOF SLR7RMMOM. In Section 3, the kinematic analysis for the mechanism is undertaken within three steps mainly using the kinematic mapping method, and the solutions for a given input angle are verified using both the CAD model and the prototype. Based upon the results from Section 3, a series of input angles are given and the operation modes and transitional configurations are obtained in Section 4. In Section 5, the algebraic approach is used to analyze the SLR7RMMOM again. Finally, conclusions are drawn.

[1]Corresponding author. Email: X.Kong@hw.ac.uk.

2. Description of a 1-DOF SLR7RMMOM

It is well known that the Sarrus linkage (Fig. 1(a)), which is composed of two groups of three R joints with parallel joint axes (rotational axes), is used to control the 1-DOF translation of the moving platform along a straight line with respect to the base. Since the Sarrus linkage is an overconstrained mechanism, we can insert one additional R joint between the two joints of a link to obtain a new 1-DOF single-loop 7R mechanism (Fig. 1(b))[17]. The advantages of adding one R joint to the Sarrus linkage are as follows. (a) It allows one to obtain a non-overconstrained mechanism from an over-constrained mechanism; (b) The Sarrus linkage has only one operation mode to complete one kind of task, but the new single-loop 7R mechanism has at least two operation modes with the possibility to fulfil different kinds of tasks on a sole mechanism; (c) The new single-loop 7R mechanism can switch from one mode to another without disassembly and without adding other actuator onto the mechanism. In the translational operation mode (Sarrus mode), it works as the Sarrus linkage in which the moving platform translates along a straight line (Fig. 1(b)). In the 1-DOF planar operation mode, the moving platform undergoes a 1-DOF general planar motion (Fig. 1(c)). Therefore, the above 7R mechanism is an SLR7RMMOM, which can switch from one operation mode to another one without causing any disconnection by using a break in a transition configuration.

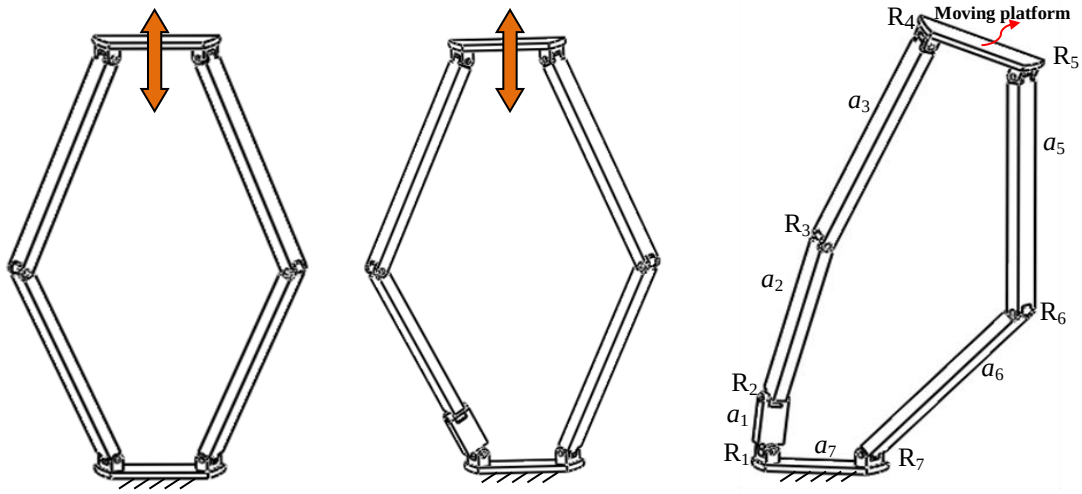
In this SLR7RMMOM, link 7 is the base, and link 4 is specified as the moving platform. Links 4 and 7 are identical and the link lengths and the axes of the R joints satisfy the following conditions:

$$\mathbf{R}_1//\mathbf{R}_3//\mathbf{R}_4\perp\mathbf{R}_2, \tag{1}$$

$$\mathbf{R}_5//\mathbf{R}_6//\mathbf{R}_7, \tag{2}$$

$$a_1+a_2=a_3=a_5=a_6 \tag{3}$$

where $\mathbf{R}_i$ (i=1,2, …,7) is the unit vector along the axis of joint R_i, and a_i is the link length as indicated in Fig. 1(c).



(a) Sarrus linkage

(b) SLR7RMMOM in translation mode (equivalent to Sarrus linkage)

(c) SLR7RMMOM in 1-DOF planar mode

Fig. 1. Construction of the SLR7RMMOM

Whether the SLR7RMMOM has additional operational modes except the two operation modes already known is unclear from only the construction of the mechanism. In the next section, we will discuss the kinematic analysis of the SLR7RMMOM in order to identify all of its operation modes as well as transitional configurations that the mechanism can switch from one operation mode to another.

3. Kinematic Analysis and Numerical Example

Using the approach to the inverse kinematics for the general 6R mechanism, [11-13] one can perform the kinematic analysis of the SLR7RMMOM. Then all the operation modes and transition configurations of the mechanism can be identified.

3.1. D-H Parameters for the mechanism

In order to define the transformation relations between the links, a coordinate frame Σ_i is attached to link i as follows: the z_i-axis coincides with the axis of joint R_i, the x_i-axis aligns with the common perpendicular to the z_{i-1}-axes and z_i-axes, and the y_i-axis is defined by the right-hand rule. With this notation one could write the transformation matrix ($\boldsymbol{T}_i$) from Σ_i to Σ_{i+1} as:

$$\boldsymbol{T}_i = \boldsymbol{M}_i\boldsymbol{G}_i = \begin{bmatrix} 1 & 0 & 0 & 0 \\ 0 & \cos(\theta_i) & -\sin(\theta_i) & 0 \\ 0 & \sin(\theta_i) & \cos(\theta_i) & 0 \\ 0 & 0 & 0 & 1 \end{bmatrix} \begin{bmatrix} 1 & 0 & 0 & 0 \\ a_i & 1 & 0 & 0 \\ 0 & 0 & \cos(\alpha_i) & -\sin(\alpha_i) \\ d_i & 0 & \sin(\alpha_i) & \cos(\alpha_i) \end{bmatrix} \tag{4}$$

where θ_i and d_i are the revolute angle and distance between the two x-axes of links i and i+1, respectively, and α_i and a_i are the twist angle and distance between the two z-axes of links i and i+1, respectively (Fig. 2).

The SLR7RMMOM can be regarded as a 6R serial mechanism (Fig. 3(a)) with link 6 as the end-effector (EE), the coordinate frame on which is set as follows. Its z-axis (z_{EE}) coincides with the axis of joint R_7 and its x-axis aligns with the common perpendicular to the z_6-axis and the z_{EE}-axis. The angle between the x_{EE}-axis and the vertical line (θ) is defined as the input angle of the SLR7RMMOM (Fig. 3(b)). The D-H parameters of the 6R mechanism are shown in Table 1, which should satisfy the conditions given in Section 2.

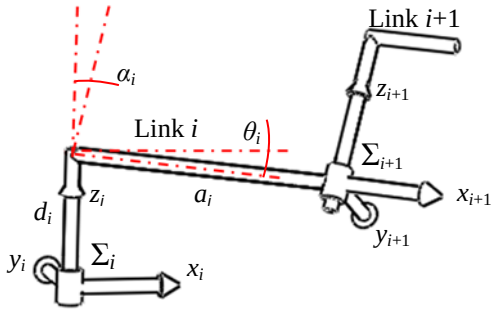
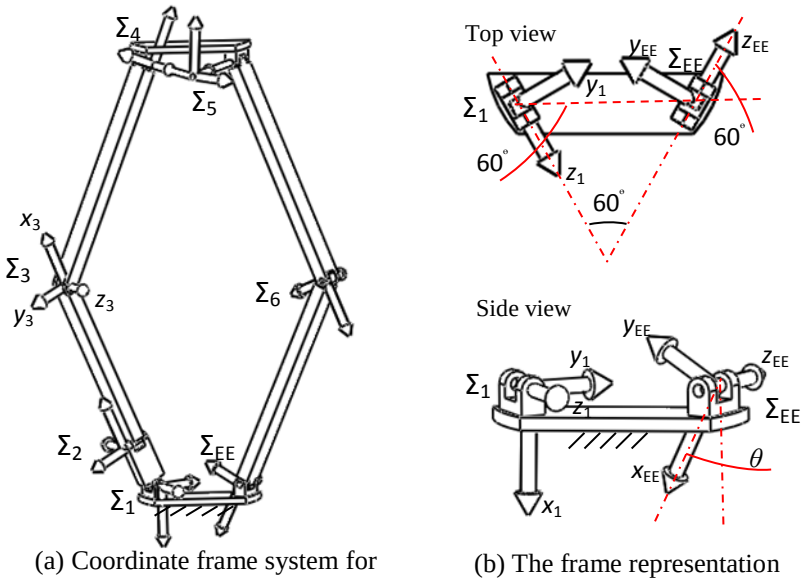


Fig. 2. D-H parameters (Σ is the coordinate frame system)

Table 1. D-H parameters for the SLR7RMMOM

i	a_i	d_i	α_i	θ_i
1	0.80	0	90°	θ_1
2	3.00	0	-90°	θ_2
3	3.80	0	0°	θ_3
4	0	1.47	-120°	θ_4
5	3.80	1.47	0°	θ_5
6	3.80	0	0°	θ_6



(a) Coordinate frame system for the SLR7RMMOM

(b) The frame representation for Σ_1 and Σ_{EE}

)

Fig. 3. Coordinate frame system for the SLR7RMMOM

In addition, the angle between the axes of joints R_1 and R_7 is 60°, θ is specified as -45° and a_7 is 1.47 (note: throughout this paper, all rotational angles are defined to be positive if the rotation is a clockwise direction about the z-axis). Therefore, the pose of end-effector Σ_{EE} with respect to Σ_1 ($\boldsymbol{A}$) can be obtained (Fig. 3(b)). First, the frame Σ_1 rotates 60° about the x-axis ($\boldsymbol{R}_1$),

then it translates 1.47 units along the *z*-axis ($\boldsymbol{P}_2$) and rotates another 60° about its *x* axis ($\boldsymbol{R}_3$), finally we get the frame Σ_{EE} after rotating -45° about the *z*-axis ($\boldsymbol{R}_4$):

$$\boldsymbol{A} = \boldsymbol{R}_1 \cdot \boldsymbol{P}_2 \cdot \boldsymbol{R}_3 \cdot \boldsymbol{R}_4 \tag{5}$$

that is:

$$\boldsymbol{A} = \begin{bmatrix} 1 & 0 & 0 & 0 \\ 0 & 0.7071067810 & 0.7071067810 & 0 \\ -1.273057344 & 0.3535533905 & -0.3535533905 & -0.8660254040 \\ 0.7350000000 & -0.6123724358 & 0.6123724358 & -0.50000000000 \end{bmatrix}.$$

3.2. Solutions for the kinematic analysis

The algorithm for the inverse kinematics analysis of a general 6R serial manipulator presented in[11-13] mainly used kinematic mapping method. Using this method, a Euclidean displacement can be mapped into a point on a study quadric (S_6^2) in a seven dimensional space, the so called kinematic mapping space P^7, where the point is displayed by eight study parameters. In the kinematic mapping space, the constraint manifold of a 2R-chain is the intersection of a 3-space with the S_6^2, and the constraint manifold of a 3R chain is the intersection of a set of 3-spaces with the S_6^2, where the set of 3-spaces is called Segre Manifold (*SM*)[11]. The *SM* of a 3R-chain can be represented by a set of four bilinear equations in the eight homogenous study parameters, which is denoted by z_0, z_1, …, z_7, and one additional parameter corresponding to the tangent half of one joint angle out of the three joint angles. That means that there are three *SMs* (SM_i, i=1, 2, 3) which are presented by three sets of four equations for a 3R-chain.

The 6R serial mechansim associated with the 1-DOF SLR7RMMOM is further decomposed into two 3R chains, the left 3R one (1-2-3) with end effector frame Σ_L and the right 3R one (6-5-4) with end effector frame Σ_R (Fig. 4). The pose of the frame Σ_L with respect to Σ_1 ($\boldsymbol{T}_L$) and the pose of the frame Σ_R with respect to Σ_1 ($\boldsymbol{T}_R$) can be obtained based on Eqs. (4) and (5):

$$\boldsymbol{T}_L = \boldsymbol{M}_1\boldsymbol{G}_1\boldsymbol{M}_2\boldsymbol{G}_2\boldsymbol{M}_3\,\boldsymbol{G}_3 \tag{6.a}$$

$$\boldsymbol{T}_R = \boldsymbol{A}\boldsymbol{G}_6^{-1}\boldsymbol{M}_6^{-1}\boldsymbol{G}_5^{-1}\boldsymbol{M}_5^{-1}\boldsymbol{G}_4^{-1}\boldsymbol{M}_4^{-1} \tag{6.b}$$

In the mechanism, the frames Σ_L and Σ_R have to coincide, which means there is intersection among SM_L, SM_R and S_6^2. The equations for the *SMs* can be derived from Eq. (6). Three sets of four equations can be obtained for the left or the right 3R chain, and each depends on one out of three joint angles[14]. One needs to select one of the three sets of four equations for the left 3R-chain and one of the three sets of four equations for the right 3R-chain according to different situations[14] before doing further calculation.

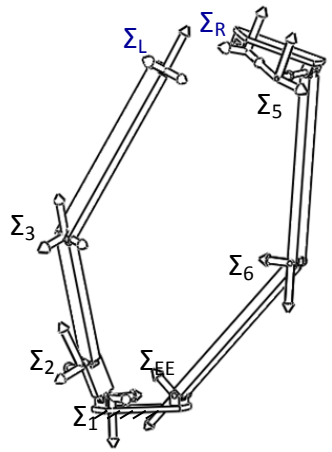


Fig. 4. Decomposing the 6R serial mechanism into two 3R chains

In some cases, not all the three *SM*s can be selected [13]. If one selects one *SM* depending on one R joint with the joint axes of the remaining two parallel or intersected, in which case the *SM* lies on the S_6^2, then the intersection of the *SM* with the S_6^2 fails. Therefore, we select SM_3, which refers to four equations in v_3 (tangent half of θ_3), for the left 3R-chain since the axes of joints R_1 and R_3 are parallel in the translational mode. For the right 3R-chain, we select SM_5 with four equations in $\bar{v}_5$ (minus tangent half of θ_5), because the axes of joints R_4 and R_5 intersect and the axes of joints R_5 and R_6 are parallel. Thus eight equations for the 6R serial mechanism are obtained as follows:

$$h1_{v_3}: 30.4z_0 + 24.0z_1 + 6.4z_2v_3 - 8.0z_4 + 8.0z_5 - 8.0z_6v_3 - 8.0z_7v_3 = 0 \tag{7}$$

$$h2_{v_3}: 30.4z_0 - 24.0z_1 - 6.4z_2v_3 + 8.0z_4 + 8.0z_5 - 8.0z_6v_3 + 8.0z_7v_3 = 0 \tag{8}$$

$$h3_{v_3}: 6.4z_1v_3 - 24.0z_2 - 30.4z_3 - 8.0z_4v_3 + 8.0z_5v_3 + 8.0z_6 + 8.0z_7 = 0 \quad (9)$$

$$h4_{v_3}: -6.4z_1v_3 + 24.0z_2 + 30.4z_3 + 8.0z_4v_3 + 8.0z_5v_3 + 8.0z_6 - 8.0z_7 = 0 \quad (10)$$

$$h5_{\bar{v}_5}: z_0(2.72626795828513 - 6.58179306856969\bar{v}_5) + z_1(4.12012622455083 - 4.85463523903963\bar{v}_5) + z_2(8.65463523574647 - 5.69413776088330\bar{v}_5) + z_3(-1.37687417023358^{-9} + 4.47457271235407^{-9}\bar{v}_5) + z_4(-1.24264068742686 - 3.00000000128678\bar{v}_5) + z_5(0.717438935080522 + 1.73205080649897\bar{v}_5) + z_6(1.73205080649897 - 0.717438935080522\bar{v}_5) + z_7(3.00000000128678 - 1.24264068742628\bar{v}_5) = 0 \quad (11)$$

$$h6_{\bar{v}_5}: z_0(-2.7262679415240 + 6.58179306736930\bar{v}_5) + z_1(0.972103152392334 + 2.74536476831045\bar{v}_5) + z_2(8.65463523588648 + 5.69413776432743\bar{v}_5) + z_3(3.07322256531961^{-9} + 1.01209529645985^{-9}\bar{v}_5) + z_4(-0.414213562192757 - 0.999999999133379\bar{v}_5) + z_5(-0.717438935213303 - 1.73205080788068\bar{v}_5) + z_6(1.73205080788068 - 0.717438935213303\bar{v}_5) + z_7(-0.99999999133379 + 0.414213562192757\bar{v}_5) = 0 \quad (12)$$

$$h7_{\bar{v}_5}: z_0(1.37687550250121^{-9} - 4.47457315644328^{-9}\bar{v}_5) + z_1(-8.65463523574647 - 5.69413776088330\bar{v}_5) + z_2(-4.12012622455083 + 4.85463523903963\bar{v}_5) + z_3(2.72626795828513 - 6.58179306856969\bar{v}_5) + z_4(-3.00000000128678 + 1.24264068742628\bar{v}_5) + z_5(1.73205080649897 - 0.717438935080522\bar{v}_5) + z_6(-0.717438935080522 - 1.73205080649897\bar{v}_5) + z_7(-1.24264068742686 - 3.00000000128678\bar{v}_5) = 0 \quad (13)$$

$$h8_{\bar{v}_5}: z_0(-3.07322167714119^{-9} - 1.01209551850445^{-9}\bar{v}_5) + z_1(8.65463523588648 + 5.69413776432743\bar{v}_5) + z_2(-0.972103152392334 - 2.74536476831045\bar{v}_5) + z_3(-2.7262679415240 + 6.58179306736930\bar{v}_5) + z_4(0.99999999133379 - 0.414213562192757\bar{v}_5) + z_5(1.73205080788068 - 0.717438935213303\bar{v}_5) + z_6(0.717438935213303 + 1.73205080788068\bar{v}_5) + z_7(-0.414213562192757 - 0.999999999133379\bar{v}_5) = 0 \quad (14)$$

$$h9: z_0z_4 + z_1z_5 + z_2z_6 + z_3z_7 = 0 \quad (15)$$

Including the equation for the S_6^2 shown in Eq. (15), we obtain nine bilinear equations in ten unknowns (Eqs. (7)-(15)). Because z_0, z_1, …, and z_7 are homogeneous, one of them can be normalize to 1. Solving seven of the nine equations to get the eight study parameters for z_0, z_1, …, z_7 in v_3 and $\bar{v}_5$, and substituting the solutions into the remaining two equations, we obtain two equations in v_3 and $\bar{v}_5$ named $E1$ and $E2$ as

$$E1: {v_3}^4{\bar{v}_5}^4 + 3.640783761{v_3}^4{\bar{v}_5}^3 - 3.788653411{v_3}^3{\bar{v}_5}^4 - 7.000053530{v_3}^4{\bar{v}_5}^2 + 10.71593007{v_3}^3{\bar{v}_5}^3 + 41.87086614{v_3}^2{\bar{v}_5}^4 + 3.640783761{v_3}^4\bar{v}_5 - 19.64341956{v_3}^2{\bar{v}_5}^3 - 3.788653411v_3{\bar{v}_5}^4 - 0.5952224873{v_3}^4 - 10.71593007{v_3}^3\bar{v}_5 - 79.84271214{v_3}^2{\bar{v}_5}^2 + 10.71593007v_3{\bar{v}_5}^3 + 11.40205846{\bar{v}_5}^4 + 3.788653411{v_3}^3 - 19.64341956{v_3}^2\bar{v}_5 - 23.28420332{\bar{v}_5}^3 + 53.83503480{v_3}^2 - 10.71593007v_3\bar{v}_5 - 131.7802740{\bar{v}_5}^2 + 3.788653411v_3 - 23.28420332\bar{v}_5 + 24.96144960 = 0 \quad (16)$$

$$E2: {v_3}^8{\bar{v}_5}^6 - 3.975059020{v_3}^8{\bar{v}_5}^5 - 9.917459999{v_3}^7{\bar{v}_5}^6 + 4.782767392{v_3}^8{\bar{v}_5}^4 + 10.89653630{v_3}^7 - 7.905713714{v_3}^6{\bar{v}_5}^6 - 2.187051780{v_3}^8{\bar{v}_5}^3 + 10.76914366{v_3}^7{\bar{v}_5}^4 + 11.58607438{v_3}^6{\bar{v}_5}^5 - 1.756500002{v_3}^5{\bar{v}_5}^6 + 0.1775892990{v_3}^8{\bar{v}_5}^2 - 6.718456391{v_3}^8 - 19.63855979{v_3}^6{\bar{v}_5}^4 - 3.599595703{v_3}^5{\bar{v}_5}^5 + 5.541460022{v_3}^4{\bar{v}_5}^6 + 0.1309074494{v_3}^8\bar{v}_5 - 10.68103759{v_3}^7{\bar{v}_5}^2 + 29.42980884{v_3}^6{\bar{v}_5}^3 + 88.38390043{v_3}^5{\bar{v}_5}^4 + 14.52156887{v_3}^4{\bar{v}_5}^5 - 11.11952017{v_3}^3{\bar{v}_5}^6 - 0.02663720154{v_3}^8 + 8.366957525{v_3}^7\bar{v}_5 + 1.744100557{v_3}^6{\bar{v}_5}^2 - 11.42375341{v_3}^5{\bar{v}_5}^3 + 47.03555747{v_3}^4{\bar{v}_5}^4 + 27.82871185{v_3}^3{\bar{v}_5}^5 + 23.16294757{v_3}^2{\bar{v}_5}^6 - 1.555454321{v_3}^7 - 14.97543807{v_3}^6\bar{v}_5 - 65.86121591{v_3}^5{\bar{v}_5}^2 + 22.54006617{v_3}^4{\bar{v}_5}^3 + 85.76873039{v_3}^3{\bar{v}_5}^4 - 19.01000389{v_3}^2{\bar{v}_5}^5 - 19.28048017v_3{\bar{v}_5}^6 + 4.289038591{v_3}^6 - 39.78294461{v_3}^5\bar{v}_5 - 55.12245682{v_3}^4{\bar{v}_5}^2 - 45.28245200{v_3}^3{\bar{v}_5}^3 + 12.06466530{v_3}^2{\bar{v}_5}^4 + 42.32484385v_3{\bar{v}_5}^5 + 8.715773829{\bar{v}_5}^6 - 4.399164900{v_3}^5 - 61.91885268{v_3}^4\bar{v}_5 - 206.5453764{v_3}^3{\bar{v}_5}^2 - 104.7180132{v_3}^2{\bar{v}_5}^3 + 8.153973623v_3{\bar{v}_5}^4 - 17.97043737{\bar{v}_5}^5 + 7.841437590{v_3}^4 - 127.7979408{v_3}^3v_3 - 166.3482520{v_3}^2{\bar{v}_5}^2 - 40.57715498v_3{\bar{v}_5}^3 - 59.39221935{\bar{v}_5}^4 - 2.488637296{v_3}^3 - 46.57694731{v_3}^2\bar{v}_5 - 151.3651980v_3{\bar{v}_5}^2 - 95.64121876{\bar{v}_5}^3 + 8.367254171{v_3}^3 - 79.64803864v_3\bar{v}_5 - 109.6592839{\bar{v}_5}^2 + 0.3550732836v_3 + 0.2355598536\bar{v}_5 + 4.481492373 = 0 \quad (17)$$

Using the "resultant" command in Maple to eliminate $\bar{v}_5$ from Eqs. (16) and (17), one polynomial equation of degree 56 in v_3 named E can be derived as follows:

$$E: ({v_3}^2 + 1)^6(3.033362327{v_3}^4 - 12.05533640{v_3}^2 + 10.67784416)(1.87522003{v_3}^4 - 64.00268390{v_3}^2 - 387.9596900)(5.157957061 \times 10^9{v_3}^{10} + 1.823061353 \times 10^{20}{v_3}^9 - 7.297142808 \times 10^{21}{v_3}^8 + 1.634647033 \times 10^{22}{v_3}^7 + 5.885504960 \times 10^{22}{v_3}^6 - 3.150969451 \times 10^{22}{v_3}^5 - 2.671416502 \times 10^{23}{v_3}^4 - 2.874236074 \times 10^{22}{v_3}^3 + 1.076318546 \times 10^{23}{v_3}^2 + 1.893149796 \times 10^{22}v_3 + 1.422425962 \times 10^{23})^2(6.60154501 \times 10^8{v_3}^{16} + 2.698070325 \times$$

$$10^{18}{v_3}^{15} - 3.778024642 \times 10^{28}{v_3}^{14} - 8.52528086 \times 10^{37}{v_3}^{13} + 6.145569255 \times 10^{47}{v_3}^{12} - 4.007107158 \times 10^{49}{v_3}^{11} + 2.109260812 \times 10^{50}{v_3}^{10} + 3.306274920 \times 10^{49}{v_3}^{9} + 5.471487282 \times 10^{50}{v_3}^{8} + 1.795904346 \times 10^{51}{v_3}^{7} - 1.709576046 \times 10^{50}{v_3}^{6} - 2.604353812 \times 10^{50}{v_3}^{5} - 8.358864852 \times 10^{50}{v_3}^{4} - 1.755833276 \times 10^{51}{v_3}^{3} + 2.679828670 \times 10^{50}{v_3}^{2} + 2.273726304 \times 10^{5}v_3 - 1.982814399 \times 10^{49}) = 0 \quad (18)$$

The solutions to $({v_3}^2 + 1)^6 = 0$ are $v_3 = \pm I$ (I is the unit imaginary number). The corresponding points in P^7 lie on the exceptional generator, which have to be cut out of the S_6^2. The solutions of polynomial of 10 degrees squared are points with coordinate (0, 0, 0, 0, 0, 0, 0, 0), which do not lie on the S_6^2 and the solutions of polynomials of degree 4 are points lie on the exceptional 3-space of the S_6^2. [13] Then the polynomial of degree 16 gives the following 16 solutions:

$$v_3 = [0.08366283786,\ 0.3610109062,\ 1.000000000,\ 6.521970015,\ 59.40599134,\ 4.132441204\times 10^9,\ 5.081725257\times 10^9,\ 0.4234204659+2.169839731\,I,\ -0.07511185210+1.019253419\,I,\ -6.650597562\times 10^9+3.156689159\times 10^8\,I,\ -0.3581658035,\ -1.000000001,\ -1.507896627,\ -6.650597562\times 10^9-3.156689159\times 10^8\,I,\ -0.07511185210-1.019253419\,I,\ 0.4234204659-2.169839731\,I] \quad (19)$$

Then the solutions for v_3 (Eq. (19)) are substituted back to $E1$ and $E2$, the common solutions for $\bar{v}_5$ with their corresponding v_3 are the solutions as desired. Please note only 12 sets of solutions could be easily obtained where the remaining four solutions for v_3 tend to be infinite, such as 5.081725257×10^9, i.e. θ_3 approaches to be 180°. The situation that θ_3=180° does exist when the joints on the platform and the base coincide. It is a special configuration for the 1-DOF SLR7RMMOM, as shown in Fig. 5(i).

The remaining four joint angles for the normal 12 sets of solutions could be solved by the other sets of four equations for SM_1, SM_2, SM_4 and SM_6.

As to the above four particularly configurations in which v_3 tend to be infinite, there is one set of real solutions: θ_2=0°, θ_3=180°, θ_6=180°, θ_1, θ_4 and θ_5 can be any value. This set of solutions can be easily verified by observation. The complex solutions associated with the remaining three particularly configurations are omitted in this paper.

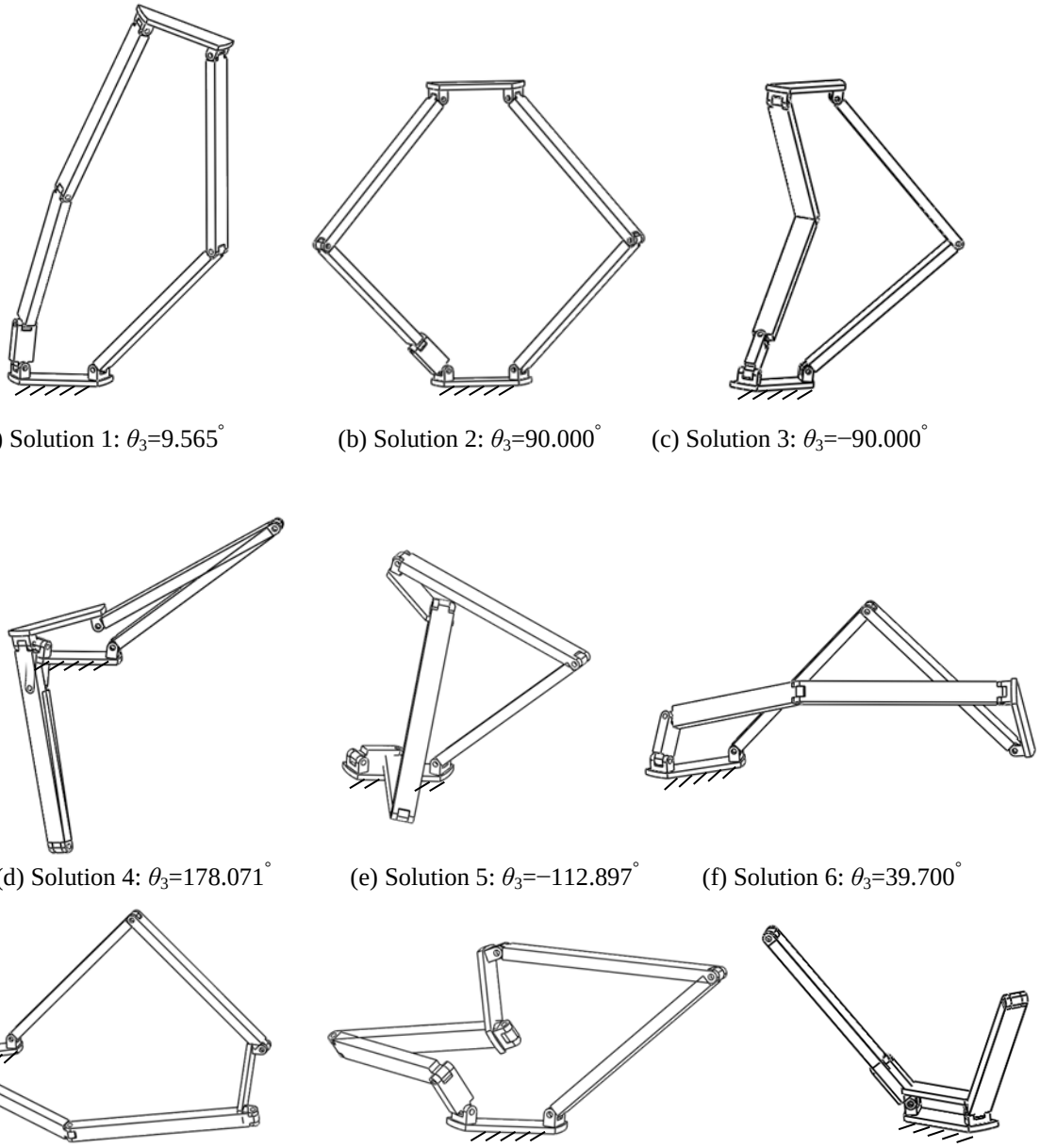
Finally, 13 sets of solutions for the kinematic analysis of the single loop are obtained, as listed in Table 2.

Table 2. Solutions for the SLR7RMMOM (Case θ=-45°)

Solutions	θ_1(deg)	θ_2(deg)	θ_3(deg)	θ_4(deg)	θ_5(deg)	θ_6(deg)
Solution 1	−173.940	20.726	9.565	−3.504	−155.426	−45.598
Solution 2	135.000	0.000	90.000	−45.000	−135.000	−90.000
Solution 3	−135.000	0.000	−90.000	45.000	−135.000	−90.000
Solution 4	−4.576	15.737	178.071	−2.648	−70.339	−172.852
Solution 5	−78.354	118.963	−112.897	−145.457	86.692	−119.924
Solution 6	−154.651	73.117	39.700	−14.351	131.208	90.703
Solution 7	−25.162	72.737	−39.412	−165.750	−41.899	90.473
Solution 8	141.385	−94.455	162.566	158.819	156.631	−137.538
Solution 9	−54.493−109.370*I*	163.879+10.798*I*	−106.507−186.806*I*	−127.985+77.436*I*	58.785+82.626*I*	−100.688−144.387*I*
Solution 10	−54.493+109.370*I*	163.879−10.798*I*	−106.507+186.806*I*	−127.985−77.436*I*	58.785−82.626*I*	−100.688+144.387*I*
Solution 11	93.401+63.964*I*	−142.300+1.679*I*	167.711+54.093*I*	105.690+9.871*I*	112.781+77.655*I*	−156.361−28.617*I*
Solution 12	93.401−63.964*I*	−142.300−1.679*I*	167.711−54.093*I*	105.690−9.871*I*	112.781−77.655*I*	−156.361+28.617*I*
Solution 13	Any value	0.000	180.000	Any value	Any value	180.000

Note: *I* is the unit imaginary number

The above real solutions for the kinematic analysis have been verified using the CAD models for the 1-DOF SLR7RMMOM. The CAD configurations associated with these solutions are shown in Fig. 5.



(a) Solution 1: θ_3=9.565° (b) Solution 2: θ_3=90.000° (c) Solution 3: θ_3=−90.000°

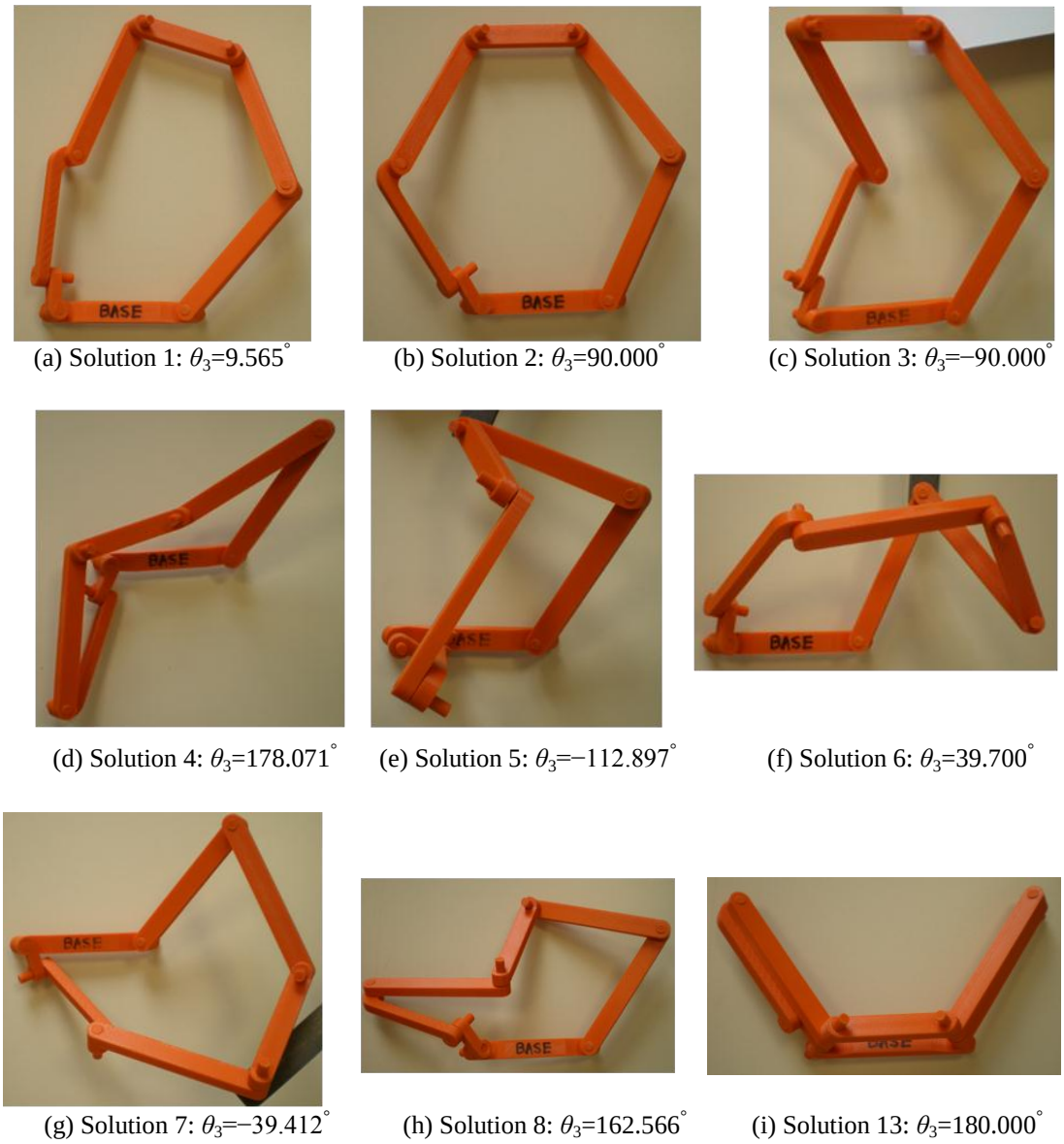
(d) Solution 4: θ_3=178.071° (e) Solution 5: θ_3=−112.897° (f) Solution 6: θ_3=39.700°

(g) Solution 7: θ_3=−39.412° (h) Solution 8: θ_3=162.566° (i) Solution 13: θ_3=180.000°

Fig. 5. CAD configurations corresponding to the real solutions for the SLR7RMMOM (Case θ=−45°)

3.3. Building prototype

A physical prototype has been built to verify the real solutions obtained above. Figure 6 illustrates that different configurations of the prototype corresponding to the real solutions can be achieved. It is noted that some configuration cannot be continuously generated in practice because of the interference between the links, such as configurations (e) and (g) (Figs. 6(e) and 6(g)).



(a) Solution 1: θ_3=9.565° (b) Solution 2: θ_3=90.000° (c) Solution 3: θ_3=−90.000°

(d) Solution 4: θ_3=178.071° (e) Solution 5: θ_3=−112.897° (f) Solution 6: θ_3=39.700°

(g) Solution 7: θ_3=−39.412° (h) Solution 8: θ_3=162.566° (i) Solution 13: θ_3=180.000°

Fig. 6. Prototype configurations corresponding to the real solutions for the SLR7RMMOM (Case θ=−45°)

4. Operation Modes and Transitional Configurations

As the input angle θ changes, a series of solutions corresponding to different input angles can be obtained accordingly using the numerical method proposed before. Then via plotting the joint angles against the input angle, we illustrate the operation modes and transitional configurations of the 1-DOF SLR7RMMOM (Fig. 7). All the operation modes and transitional configurations of the mechanism can be obtained from the plotting of angles θ_1 and θ_3 against the input angle θ.

Figure 7 shows that there are two straight lines A and B and two closed curves C (C_0-C_1-C_2-C_0 in Fig. 7(a) or C_0-C_1-C_2-C_3-C_4-C_0 in Fig. 7(b)) and D (D_0-D_1-D_2-D_3-D_4-D_0) designating the operations modes. Lines A and B are associated with translation operation mode, while the closed curves C and D are associated with two 1-DOF planar operation modes separately. Therefore, the mechanism has three operation modes but not only two operation modes. This can be easily verified by comparing the straight lines and closed curves to their corresponding operation mode figures in Fig. 5. Line A corresponds to Fig. 5(b), Line B corresponds to Fig. 5(c), closed curve C corresponds to Fig. 5(a), and closed curve D corresponds to Fig. 5(g). Points 1, 2, …, 8 in Fig. 7 indicate the eight real solutions for θ_3 (or θ_1) under θ=−45° corresponding to Table 2 except the special solution for θ_3=180° (Fig. 6(i)).

In the following, the transitional configurations between three operation modes are analyzed. By comparing the two plotting figures, Fig. 7(a) and Fig. 7(b), two intersecting points TA and TB through which both operation modes pass in both the plotting figures are apparently observed, which represent the two transitional configurations (Fig. 8). The input angles corresponding to the transitional configurations are shown in Table 3.

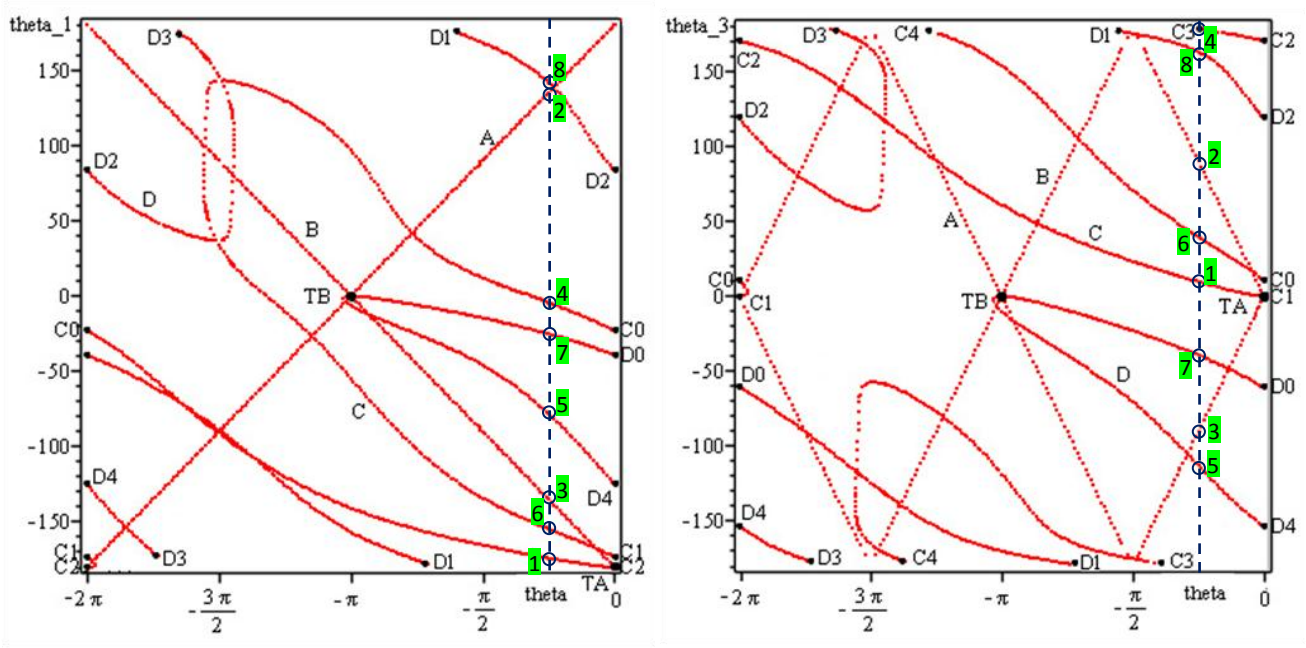
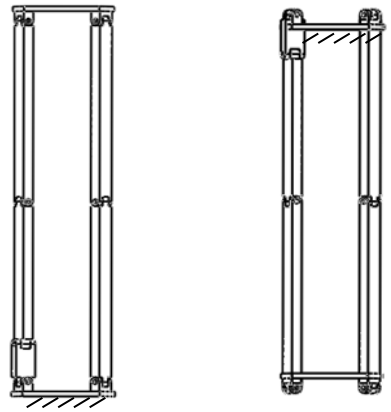


Fig. 7. Plotting of two rotational angles (θ_1 and θ_3) against input angle θ: a) θ_1 (deg) in vertical axis versus θ (rad) in the horizontal axis; b) θ_3 (deg) in vertical axis versus θ (rad) in the horizontal axis

Table 3. Transitional configurations

Transition points	Input angle θ in degree	Modes
TA	0°	Translational mode & 1-DOF planar mode I (curve C)
TB	-180°	Translational mode & 1-DOF planar mode II (curve D)



(a) TA: $\theta=0^\circ$ (b) TB: $\theta=-180^\circ$

Fig. 8. Transitional configurations of the SLR7RMMOM

5. Algebraic Approach

In this section, the algebraic approach proposed in [15] will be applied to figure out the operation modes and transitional configurations. Apparently, compared to the above numerical method (Section 4), the algebraic approach enables the operation modes to be represented algebraically.

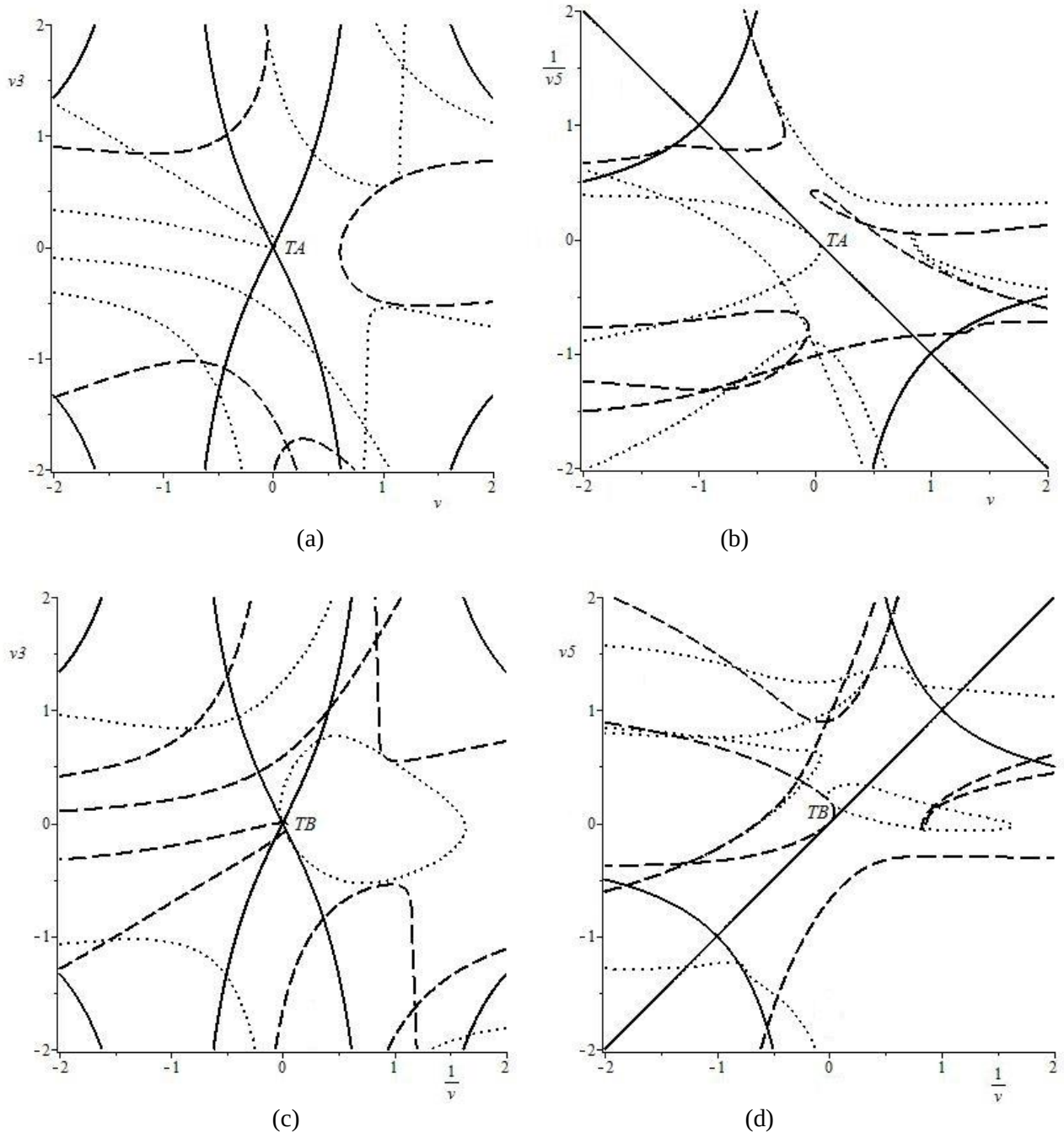


Fig. 9. Plots of the input output equations using algebraic approach

Without specifying the input angle like shown in Section 3, we present the end-effector pose $\boldsymbol{A}$ and the equations for $\boldsymbol{SM}_i$ directly in θ. Therefore nine equations in v_3 (tangent half of θ_3), $\bar{v}_5$, (minus tangent half of θ_5), v (tangent half of θ) and eight study parameters (Eqs. (7)-(15)) can be obtained. Two equations in v_3, $\bar{v}_5$ and v instead of two equations in v_3 and $\bar{v}_5$ will be obtained after solving seven of the nine equations and substituting the solutions into the remaining two equations. Using the "resultant" function in Maple to eliminate $\bar{v}_5$ (or v_3), then we get the bivariate polynomial in the input angle v and one of the remaining joint parameter v_3 (or $\bar{v}_5$). Beside some spurious factors, there are three factors corresponding to three operation modes respectively. For example, the input-output equation in v_3 and v is:

$$S \cdot M1 \cdot M2 \cdot M3 = 0 \tag{20}$$

where S is a spurious factor. M1 is the input-output relation corresponding to the translational mode, while M2 and M3 represent the two general planar modes, respectively (see the Appendix for the detailed expressions).

Then we can plot the input-output relation in v_3 and v (Fig. 9(a)), which shows three operation modes along with one transitional configuration. The solid curve corresponds to the translational mode, the dotted curve corresponds to the planar mode I and the dashed curve corresponds to planar mode II.

The numerical method is still kept in this paper even though it is not as simple or effective as the algebraic approach since it indicates all the results directly and clearly. The plots for the input-output angles in Fig. 7 show that there are two transitional configurations: (a) the input angle θ=0°, the revolute angles θ_3=0° and θ_5=180°; (b) the input angle θ=−180°, the revolute angles θ_3=0° and θ_5=0°. When the input angle θ=−180°, v tends to be infinite. Therefore the second transitional configuration cannot be seen directly from the plot of the input-output relation in v and v_3 (or v_5) in Fig. 9(a) using the algebraic approach. Then we have to use the reciprocal of variables to plot the relations in v and $1/v_5$, $1/v$ and v_3 as well as the relation in $1/v$ and v_5 (Fig. 9) so that all transitional configurations can be observed. In Fig. 9, the transition between the translation mode and planar mode I is TA, and the translation mode and planar mode II are transited at TB. It has been shown that the algebraic analysis results are the same as the numerical ones shown in Section 4 as expected.

6. Conclusions

This paper has presented a novel 1-DOF single-loop reconfigurable 7R mechanism with multiple operation modes (SLR7RMMOM) base on the Sarrus mechanism. The kinematics analysis of the novel SLR7RMMOM has been implemented using the algorithm for the inverse kinematics of a general serial 6R manipulator, which is very effective. Using a numerical method, a set of solutions for the 1-DOF SLR7RMMOM have been obtained for a given example and the real solutions have been verified through both the CAD model and the prototype of the mechanism. In addition, the numerical method and an algebraic approach have been both applied to obtain the operation modes and transitional configurations, which produce the same results. The mechanism has three operation modes: translational mode and two 1-DOF planar modes, and there are two transitional configurations where the mechanism can switch from one operation mode to another.

The SLR7RMMOM on one hand is a non-overconstrained system, and on the other hand can switch from one mode to another without disassembly and without using additional actuator, which can help develop energy-efficient reconfigurable mechanisms. The work proposed in this paper contributes to the design and analysis of new mechanical systems with multiple operation modes.

Acknowledgements

The authors would like to acknowledge the Royal Society, United Kingdom for the financial support through an International Joint Project No. JP100715. X. He would like to acknowledge the financial support from the SORSAS PhD scholarship in Heriot-Watt University. Special thanks go to Prof. M.L. Husty and Dr. M. Pfurner in Universität Innsbruck, Austria for their valuable help in using their kinematic mapping algorithms.

References

1. G. Yang, I. Chen, K.M. Lim and Y.S. Huat, "Design and kinematic analysis of modular reconfigurable parallel robots," Proceedings of *the IEEE Conference on Robotics and Automation*, Detroit, MI, US (May 1999) pp. 2501-2506.
2. G. Yang, I.-M. Chen, W. K. Lim, and S. H. Yeo, "Kinematic design of modular reconfigurable in-parallel robots," *Autonomous Robots*, **10**(1), 83-89 (2001).
3. C. Kuo and J. Dai, "Reconfiguration principles and strategies for reconfigurable mechanisms," *ASME/IFToMM International Conference on Reconfigurable Mechanisms and Robots*, London, UK (June 2009).
4. C. Galletti and P. Fanghella, "Single-loop kinematotropic mechanism," *Mechanism and Machine Theory*, **36**(6), 743-761 (2001).
5. N. Rakotomanga, D. Chablat, and S. Caro, "Kinatostatic performance of a planar mechanism with variable actuation," *Advances in Robot Kinematics: Analysis and Design*, pp. 311-320 (Springer Netherlands, 2008).
6. X. Kong and C. Huang, "Type synthesis of single-DOF single-loop mechanisms with two operation modes," *ASME/IFToMM International Conference on Reconfigurable Mechanisms and Robots*, London, UK (June 2009).
7. C. Huang, R. Tseng, and X. Kong, "Design and kinematic analysis of a multiple-mode 5R2P closed-loop linkage", *New Trends in Mechanism Science: Analysis and Design*, pp. 3-10, (Springer, Netherlands, 2010)
8. X. Kong, "Type synthesis of 3-DOF parallel manipulators with both a planar operation mode and a spatial translational operation mode,"*Journal of Mechanisms and Robotics*, 5(4), 041015 (Oct. 2013).
9. D. Zlatanov, I.A. Bonev, and C.M. Gosselin, "Constraint singularity as C-space singularities," *Advances in Robot Kinematics-Theory and Application*, pp. 183-192 (Kluwer Academic Publishers, Netherlands, 2002).
10. X. Wang, M. Hao, and Y. Cheng, "On the use of differential evolution for forward kinematics of parallel manipulators," *Applied Mathematics and Computation*, **205**(2), 760-769 (Nov. 2008).
11. I. A. Bonev, D. Zlatanov, and C.M. Gosselin, "Singularity analysis of 3-DOF planar parallel mechanisms via screw theory," *Journal of Mechanical Design*, **125**(3), 573-581 (Sep. 2003).
12. M. L. Husty, M. Pfurner, and H.P. Schrocker, "A New and effective algorithm for the inverse kinematics of a general serial 6R manipulator," *Mechanism and Machine Theory*, **42**(1): 66-81 (2007).
13. M. L. Husty, M. Pfurner, H.P. Schrocker, and K. Brunnthaler, "Algebraic method in mechanism analysis and synthesis," *Robotica*, **25**(6): 661-675 (2007).
14. M. Pfurner, *Analysis of Spatial Serial Manipulators Using Kinematic Mapping* (PhD Thesis, University of Innsbruck, Austria, 2006).

15. M. Pfurner, X. Kong, and C. Huang, "Algebraic analysis of a multiple-Mode 5R2P closed-loop linkage," *Proceedings of International Line Geometry & Kinematics*, Paphos, Cyprus (April 2011).
16. M. Pfurner, "Multiple-mode closed 7-link chains based on overconstrained 4-link mechanisms," *New Trends in Mechanism and Machine Science*, pp. 73-81 (Springer, Netherlands, 2007).
17. X. Kong and C.M. Gosselin, *Type Synthesis of Parallel Mechanisms* (Springer, Netherlands, 2007).

Appendix: Expressions of M1, M2 and M3 in Algebraic Approach

$$
\begin{aligned}
M1: &- 2.98281097610^{30}v^8v3^2 + 9.85628630510^9v^8v3^4 - 4.97462522610^{20}v - 4.97462522610^{20}v^7 \\
&+ 1.17615268310^{11}v^7v3^4 - 4.97462522410^{20}v^7v3^2 + 1.17615268310^{11}vv3^4 + 9.85628630510^9v3^4 \\
&- 1.49238756810^{21}v^5 + 2.38624878110^{31}v^4 + 1.19312439010^{31}v^6 - 4.28618394210^{11}v^3v3^4 \\
&+ 3.72958160810^{21}v^6v3^2 + 3.71617611210^{11}v^2v3^4 + 5.96562196010^{30}v^4v3^2 - 4.28618394210^{11}v^5v3^4 \\
&+ 4.85845283710^{11}v^4v3^4 + 3.71617611210^{11}v^6v3^4 - 1.49238756910^{21}v^5v3^2 + 3.72958160810^{21}v^2v3^2 \\
&- 4.97462522410^{20}vv3^2 - 1.49238756910^{21}v^3v3^2 - 2.98281097610^{30}v3^2 + 5.1434072810^8 \\
&- 1.49238756810^{21}v^3 + 1.19312439010^{31}v^2 + 5.1434072810^8v^8
\end{aligned}
\tag{A.1}
$$

$$
\begin{aligned}
M2: &- 2.31563104710^{24}v^9v3^4 - 3.71161830210^{23}v^9v3^3 - 1.36573973110^{24}v^9v3^2 - 3.43545947210^{22}v^9v3 \\
&+ 1.37816049310^{23}v^8v3 - 2.19915627110^{24}v^8v3^2 + 1.46079653810^{24}v^8v3^4 + 2.22664230910^{23}v^8v3^3 \\
&+ 1.35735210310^{24}v^{10}v3^4 + 4.35765803610^{23}v^{10}v3^3 - 2.16961505810^{24}v^{10}v3^2 + 3.20497020410^{23}v^{10}v3 \\
&+ 8.42009336010^{21}v - 1.42793175410^{22} + 9.40258182510^{23}v^7 - 1.84751221110^{24}v^7v3^4 \\
&- 4.63539161010^{23}v^7v3^3 - 1.30882918710^{24}v^7v3^2 - 1.00765919210^{23}v^7v3 - 3.49609719910^{22}vv3^4 \\
&- 4.32669291410^{22}v^6v3 + 1.66949849410^{22}v3^4 + 3.93757660510^{23}v^5 - 2.71228439610^{23}v^4 \\
&- 3.88067793810^{23}v^6 - 2.72909386810^{23}v^3v3^4 - 9.41530998510^{22}v^5v3 - 8.21972559610^{22}v^4v3 \\
&- 1.56322781510^{24}v^6v3^2 + 1.29660917310^{23}v^2v3^4 - 7.33267703510^{23}v^4v3^2 - 3.31771188510^{23}v^5v3^3 \\
&- 6.30444670010^{22}v^4v3^3 - 9.35099367110^{23}v^5v3^4 + 4.70501027710^{23}v^4v3^4 + 1.02943136310^{24}v^6v3^4 \\
&- 7.74698173010^{23}v^5v3^2 - 9.40734364210^{19}v^6v3^3 - 3.01300068810^{22}v^2v3^3 - 2.13013583510^{22}vv3^3 \\
&- 1.29175112510^{23}v^3v3^3 - 4.61516340710^{21}v3^3 - 3.77854521110^{22}v^2v3 - 7.42636498410^{21}vv3 \\
&- 4.17904870110^{22}v^3v3 - 2.01519903110^{23}v^2v3^2 - 3.71713607110^{22}vv3^2 - 2.58401761210^{23}v^3v3^2 \\
&- 2.43196391510^{22}v3^2 + 9.01320154610^{22}v^3 - 9.70825246110^{22}v^2 - 6.23543533510^{21}v3 \\
&- 2.90618229310^{23}v^8v3^6 + 9.49736270910^{22}v^7v3^7 + 3.02146030310^{22}v^6v3^8 + 3.23184214610^{23}v^{12}v3 \\
&- 9.06165074210^{23}v^{11}v3^2 - 8.45115460310^{22}v^8v3^5 + 3.49285099710^{23}v^7v3^6 - 1.23644623310^{23}v^6v3^7 \\
&- 3.66654823010^{22}v^5v3^8 + 3.39694221410^{22}v^{11}v3 - 2.65723553510^{23}v^7v3^5 - 2.40140792510^{23}v^6v3^6 \\
&+ 5.48509545210^{22}v^5v3^7 + 1.28135606510^{22}v^4v3^8 - 8.12469585910^{22}v^6v3^5 + 1.96690984010^{23}v^5v3^6 \\
&- 4.97296102710^{22}v^4v3^7 - 1.22428182110^{22}v^3v3^8 - 1.81848455710^{23}v^5v3^5 - 1.15337625110^{23}v^4v3^6 \\
&+ 1.69348942410^{22}v^3v3^7 + 2.08556862110^{21}v^2v3^8 - 3.03447419010^{22}v^4v3^5 + 6.33815715810^{22}v^3v3^6 \\
&- 8.45561805010^{21}v^2v3^7 - 1.55424043710^{21}vv3^8 - 7.03228098410^{22}v^3v3^5 - 2.89890049110^{22}v^2v3^6 \\
&+ 2.12628191410^{21}vv3^7 - 5.47856091610^{20}v^2v3^5 + 9.07624163610^{21}vv3^6 - 1.17624732310^{22}vv3^5 \\
&- 1.22293311410^{22}v^{14}v3^8 - 1.34675153710^{22}v^{14}v3^7 + 1.96383425010^{22}v^{13}v3^8 + 9.24541577310^{21}v^{14}v3^6 \\
&+ 1.98810552510^{22}v^{13}v3^7 - 1.30088157310^{22}v^{12}v3^8 + 3.75704391110^{22}v^{14}v3^5 + 8.64870773210^{22}v^{13}v3^6 \\
&- 5.96825926410^{22}v^{12}v3^7 + 6.37264899010^{21}v^{11}v3^8 + 2.76918552610^{23}v^{14}v3^4 - 4.12365625610^{22}v^{13}v3^5 \\
&- 6.49107912610^{22}v^{12}v3^6 + 5.75748361010^{22}v^{11}v3^7 + 8.23347977910^{21}v^{10}v3^8 + 2.31486458910^{23}v^{14}v3^3 \\
&- 9.93161171810^{23}v^{13}v3^4 + 3.86484990310^{22}v^{12}v3^5 + 2.47198525910^{23}v^{11}v3^6 - 1.32091607110^{23}v^{10}v3^7 \\
&- 3.11698666510^{22}v^9v3^8 - 7.45073915110^{23}v^{14}v3^2 - 1.73719638810^{22}v^{13}v3^3 + 8.01166962010^{23}v^{12}v3^4 \\
&- 1.32398335510^{23}v^{11}v3^5 - 2.02799792710^{23}v^{10}v3^6 + 9.59853819210^{22}v^9v3^7 + 3.18860317210^{22}v^8v3^8 \\
&+ 1.81109563210^{23}v^{14}v3 - 3.77514994610^{23}v^{13}v3^2 + 4.21489122210^{23}v^{12}v3^3 - 1.89537531510^{24}v^{11}v3^4 \\
&- 1.83602661710^{22}v^{10}v3^5 + 3.79078829110^{23}v^9v3^6 - 1.67371396910^{23}v^8v3^7 - 5.22900588710^{22}v^7v3^8 \\
&+ 4.30111331410^{22}v^{13}v3 - 1.52934909710^{24}v^{12}v3^2 - 1.56426611410^{23}v^{11}v3^3 - 2.38816149910^{23}v^9v3^5 \\
&+ 1.37617829410^{19}vv3^9 + 1.40679591210^{10}vv3^{10} - 2.52316725910^{20}v^2v3^9 + 1.72099194910^{10}v^2v3^{10} \\
&- 1.26921403410^{20}v^3v3^9 + 5.23527634610^{10}v^3v3^{10} + 6.01737565510^{22}v^{14} + 6.82494912010^{23}v^{13} \\
&+ 9.25287458210^{22}v^{12} + 1.23003611810^{24}v^{11} - 3.67026003510^{18}v3^8 - 1.00069526910^{19}v3^7 \\
&- 2.73201585510^{21}v3^6 + 1.66038988110^{21}v3^5 + 1.36014001210^{24}v^9 - 2.70036899310^{23}v^8 \\
&- 2.55802632710^{22}v^{10} + 1.26706946810^{22}v^{16} + 2.87468445610^{22}v^{17} + 2.11609148010^{20}v^{18} \\
&+ 2.13133206410^{23}v^{15} - 5.01249059210^{19}v3^9 + 2.73922374810^9v3^{10} + 1.79349474910^{21}v^{17}v3^8 \\
&+ 3.22401027710^{20}v^{17}v3^7 - 1.11470394210^{21}v^{17}v3^6 + 3.63140604110^{20}v^{17}v3^5 + 1.31847440210^{20}v^{17}v3^9 \\
&+ 1.60104590010^{10}v^{17}v3^{10} + 1.67197822010^{21}v^{18}v3^4 + 8.95639546510^{21}v^{18}v3^3 - 3.12108765410^{22}v^{18}v3^2 \\
&+ 7.20220601210^{21}v^{18}v3 - 2.35393568410^{20}v^{18}v3^8 + 1.53710572310^{20}v^{18}v3^7 + 3.39541819410^{21}v^{18}v3^6 \\
&+ 1.95437340910^{21}v^{18}v3^5 - 4.64733841710^{19}v^{18}v3^9 + 4.20014308110^9v^{18}v3^{10} - 6.61058806710^{20}v^{14}v3^9 \\
&- 4.50967915110^{10}v^{14}v3^{10} - 3.05077803310^{23}v^{15}v3^4 + 1.07721802910^{22}v^{15}v3^3 - 9.20953519610^{22}v^{15}v3^2 \\
&+ 1.87291069110^{22}v^{15}v3 + 1.02024759510^{22}v^{15}v3^8 + 3.68271720210^{21}v^{15}v3^7 + 1.03532309610^{22}v^{15}v3^6 \\
&- 4.85580195910^{21}v^{15}v3^5 + 5.81592542610^{20}v^{15}v3^9 + 1.48494473010^{10}v^{15}v3^{10} + 4.58754020910^{22}v^{16}v3^4 \\
&+ 6.94908549110^{22}v^{16}v3^3 - 2.24554857710^{23}v^{16}v3^2 + 5.51888357710^{22}v^{16}v3 - 3.61817966210^{21}v^{16}v3^8 \\
&- 7.12046497010^{20}v^{16}v3^7 + 1.43099054210^{22}v^{16}v3^6 + 1.39171306910^{22}v^{16}v3^5 - 3.27158040110^{20}v^{16}v3^9 \\
&- 2.63147826510^{10}v^{16}v3^{10} - 4.20221581110^{22}v^{17}v3^4 + 3.23763630310^{21}v^{17}v3^3 - 1.03671148610^{22}v^{17}v3^2 \\
&+ 3.06504928610^{21}v^{17}v3 + 1.53744231310^{21}v^{10}v3^9 + 8.34294207410^{11}v^{10}v3^{10} - 4.22861998610^{20}v^{11}v3^9 \\
&- 5.67791093710^{11}v^{11}v3^{10} - 2.61840738410^{19}v^{12}v3^9 + 2.62593482210^{11}v^{12}v3^{10} + 7.34520789610^{20}v^{13}v3^9 \\
&- 1.83896682010^{11}v^{13}v3^{10} - 2.07606121210^{21}v^7v3^9 - 3.49194514010^{11}v^7v3^{10} + 1.98833084110^{21}v^8v3^9 \\
&+ 9.68270806710^{11}v^8v3^{10} - 2.00570366310^{21}v^9v3^9 - 6.81506714810^{11}v^9v3^{10} - 2.32079409310^{20}v^4v3^9 \\
&+ 1.37277400510^{11}v^4v3^{10} - 9.18678421610^{20}v^5v3^9 - 1.44584181610^{10}v^5v3^{10} + 7.75191015610^{20}v^6v3^9 \\
&+ 5.33958652010^{11}v^6v3^{10}
\end{aligned}
\tag{A.2}
$$

$$
\begin{aligned}
M3:\ & 2.640005305\,10^{33}\,v^9 v3^4 - 1.598539782\,10^{33}\,v^9 v3^3 - 2.861873158\,10^{33}\,v^9 v3^2 + 3.342554298\,10^{32}\,v^9 v3 \\
& + 4.712020506\,10^{33}\,v^8 v3^2 - 2.535198074\,10^{33}\,v^8 v3^4 - 1.976845023\,10^{33}\,v^{10} v3^4 + 1.230826426\,10^{33}\,v^{10} v3^3 \\
& + 3.314434734\,10^{33}\,v^{10} v3^2 - 8.760836205\,10^{31}\,v^{10} v3 + 2.311427381\,10^{21}\,v - 4.950318962\,10^{21}\,v^7 \\
& + 2.640005305\,10^{33}\,v^7 v3^4 + 1.598539782\,10^{33}\,v^7 v3^3 - 2.861873158\,10^{33}\,v^7 v3^2 - 3.342554298\,10^{32}\,v^7 v3 \\
& + 7.542872295\,10^{31}\,vv3^4 + 8.760836205\,10^{31}\,v^6 v3 - 2.155613374\,10^{31}\,v3^4 + 5.614836355\,10^{21}\,v^5 \\
& - 8.847937850\,10^{31}\,v^4 - 2.211984462\,10^{32}\,v^6 + 5.280010610\,10^{32}\,v^3 v3^4 - 6.016597735\,10^{32}\,v^5 v3 \\
& + 8.760836210\,10^{31}\,v^4 v3 + 3.314434734\,10^{33}\,v^6 v3^2 - 2.237625055\,10^{32}\,v^2 v3^4 + 9.744448600\,10^{32}\,v^4 v3^2 \\
& + 2.877371606\,10^{33}\,v^5 v3^3 - 1.230826426\,10^{33}\,v^4 v3^3 + 1.584003182\,10^{33}\,v^5 v3^4 - 9.114523580\,10^{32}\,v^4 v3^4 \\
& - 1.976845023\,10^{33}\,v^6 v3^4 - 1.717123895\,10^{33}\,v^5 v3^2 - 1.230826426\,10^{33}\,v^6 v3^3 - 5.274970395\,10^{32}\,v^2 v3^3 \\
& + 3.197079563\,10^{32}\,vv3^3 + 1.598539782\,10^{33}\,v^3 v3^3 - 8.791617325\,10^{31}\,v3^3 + 3.754644091\,10^{31}\,v^2 v3 \\
& - 6.685108595\,10^{31}\,vv3 - 3.342554298\,10^{32}\,v^3 v3 - 4.671694796\,10^{31}\,v^2 v3^2 - 8.176780455\,10^{31}\,vv3^2 \\
& - 5.723746320\,10^{32}\,v^3 v3^2 - 6.273732740\,10^{31}\,v3^2 - 3.597172912\,10^{20} + 7.594963935\,10^{21}\,v^3 \\
& - 1.474656308\,10^{31}\,v^2 + 6.257740155\,10^{30}\,v3 - 7.266418520\,10^{33}\,v^8 v3^6 - 3.228957702\,10^{31}\,v^7 v3^7 \\
& - 1.273606457\,10^{33}\,v^6 v3^8 - 8.760836210\,10^{31}\,v^{12} v3 - 1.717123895\,10^{33}\,v^{11} v3^2 + 6.650075605\,10^{33}\,v^7 v3^6 \\
& - 1.906546146\,10^{31}\,v^6 v3^7 + 6.889182835\,10^{32}\,v^5 v3^8 + 6.016597735\,10^{32}\,v^{11} v3 + 1.951298274\,10^{33}\,v^7 v3^5 \\
& - 5.188109825\,10^{33}\,v^6 v3^6 - 5.812123865\,10^{31}\,v^5 v3^7 - 4.827086746\,10^{32}\,v^4 v3^8 - 1.360973320\,10^{33}\,v^6 v3^5 \\
& + 3.990045362\,10^{33}\,v^5 v3^6 - 1.906546148\,10^{31}\,v^4 v3^7 + 2.296394278\,10^{32}\,v^3 v3^8 + 3.512336893\,10^{33}\,v^5 v3^5 \\
& - 1.656517424\,10^{33}\,v^4 v3^6 - 3.228957702\,10^{31}\,v^3 v3^7 - 6.453840515\,10^{31}\,v^2 v3^8 - 1.360973320\,10^{33}\,v^4 v3^5 \\
& + 1.330015120\,10^{33}\,v^3 v3^6 - 8.170912070\,10^{30}\,v^2 v3^7 + 3.280563254\,10^{31}\,vv3^8 + 1.951298274\,10^{33}\,v^3 v3^5 \\
& - 2.684426957\,10^{31}\,v^2 v3^6 - 6.457915405\,10^{30}\,vv3^7 - 5.832742800\,10^{32}\,v^2 v3^5 + 1.900021600\,10^{32}\,vv3^6 \\
& + 3.902596548\,10^{32}\,vv3^5 - 6.453840515\,10^{31}\,v^{14} v3^8 + 8.170912070\,10^{30}\,v^{14} v3^7 + 2.296394278\,10^{32}\,v^{13} v3^8 \\
& - 2.684426957\,10^{31}\,v^{14} v3^6 + 3.228957702\,10^{31}\,v^{13} v3^7 - 4.827086746\,10^{32}\,v^{12} v3^8 + 5.832742800\,10^{32}\,v^{14} v3^5 \\
& + 1.330015120\,10^{33}\,v^{13} v3^6 + 1.906546148\,10^{31}\,v^{12} v3^7 + 6.889182835\,10^{32}\,v^{11} v3^8 - 2.237625055\,10^{32}\,v^{14} v3^4 \\
& - 1.951298274\,10^{33}\,v^{13} v3^5 - 1.656517424\,10^{33}\,v^{12} v3^6 + 5.812123865\,10^{31}\,v^{11} v3^7 - 1.273606457\,10^{33}\,v^{10} v3^8 \\
& + 5.274970395\,10^{32}\,v^{14} v3^3 + 5.280010610\,10^{32}\,v^{13} v3^4 + 1.360973320\,10^{33}\,v^{12} v3^5 + 3.990045362\,10^{33}\,v^{11} v3^6 \\
& + 1.906546146\,10^{31}\,v^{10} v3^7 + 1.148197140\,10^{33}\,v^9 v3^8 - 4.671694796\,10^{31}\,v^{14} v3^2 - 1.598539782\,10^{33}\,v^{13} v3^3 \\
& - 9.114523580\,10^{32}\,v^{12} v3^4 - 3.512336893\,10^{33}\,v^{11} v3^5 - 5.188109825\,10^{33}\,v^{10} v3^6 + 3.228957702\,10^{31}\,v^9 v3^7 \\
& - 1.720420200\,10^{33}\,v^8 v3^8 - 3.754644091\,10^{31}\,v^{14} v3 - 5.723746320\,10^{32}\,v^{13} v3^2 + 1.230826426\,10^{33}\,v^{12} v3^3 \\
& + 1.584003182\,10^{33}\,v^{11} v3^4 + 1.360973320\,10^{33}\,v^{10} v3^5 + 6.650075605\,10^{33}\,v^9 v3^6 + 1.148197140\,10^{33}\,v^7 v3^8 \\
& + 3.342554298\,10^{32}\,v^{13} v3 + 9.744448600\,10^{32}\,v^{12} v3^2 - 2.877371606\,10^{33}\,v^{11} v3^3 - 1.951298274\,10^{33}\,v^9 v3^5 \\
& - 1.015852790\,10^{31}\,vv3^9 + 4.371918688\,10^{20}\,vv3^{10} - 9.895286260\,10^{18}\,vv3^{11} + 7.445942390\,10^9\,vv3^{12} \\
& + 1.005988742\,10^{31}\,v^2 v3^9 - 4.570575250\,10^{29}\,v^2 v3^{10} + 7.418705120\,10^{19}\,v^2 v3^{11} + 2.287889851\,10^{10}\,v^2 v3^{12} \\
& - 5.079263950\,10^{31}\,v^3 v3^9 + 5.405983040\,10^{21}\,v^3 v3^{10} - 1.474656308\,10^{31}\,v^{14} + 7.594963935\,10^{21}\,v^{13} \\
& - 8.847937850\,10^{31}\,v^{12} + 5.614836355\,10^{21}\,v^{11} + 4.773912180\,10^{30}\,v3^8 - 1.361818680\,10^{30}\,v3^7 \\
& + 7.477259030\,10^{31}\,v3^6 - 9.721238000\,10^{31}\,v3^5 - 4.950318962\,10^{21}\,v^9 - 2.949312616\,10^{32}\,v^8 \\
& - 2.211984462\,10^{32}\,v^{10} - 3.597172912\,10^{20}\,v^{16} + 2.311427381\,10^{21}\,v^{15} + 1.676647904\,10^{30}\,v3^9 \\
& - 1.888346556\,10^{29}\,v3^{10} - 5.333963550\,10^9\,v3^{11} + 6.23978001\,10^8\,v3^{12} - 1.005988742\,10^{31}\,v^{14} v3^9 \\
& - 4.570575250\,10^{29}\,v^{14} v3^{10} - 7.418705120\,10^{19}\,v^{14} v3^{11} + 2.287889851\,10^{10}\,v^{14} v3^{12} + 7.542872295\,10^{31}\,v^{15} v3^4 \\
& - 3.197079563\,10^{32}\,v^{15} v3^3 - 8.176780455\,10^{31}\,v^{15} v3^2 + 6.685108595\,10^{31}\,v^{15} v3 + 3.280563254\,10^{31}\,v^{15} v3^8 \\
& + 6.457915405\,10^{30}\,v^{15} v3^7 + 1.900021600\,10^{32}\,v^{15} v3^6 - 3.902596548\,10^{32}\,v^{15} v3^5 + 1.015852790\,10^{31}\,v^{15} v3^9 \\
& + 4.371918688\,10^{20}\,v^{15} v3^{10} + 9.895286260\,10^{18}\,v^{15} v3^{11} + 7.445942390\,10^9\,v^{15} v3^{12} - 2.155613374\,10^{31}\,v^{16} v3^4 \\
& + 8.791617325\,10^{31}\,v^{16} v3^3 - 6.273732740\,10^{31}\,v^{16} v3^2 - 6.257740155\,10^{30}\,v^{16} v3 + 4.773912180\,10^{30}\,v^{16} v3^8 \\
& + 1.361818680\,10^{30}\,v^{16} v3^7 + 7.477259030\,10^{31}\,v^{16} v3^6 + 9.721238000\,10^{31}\,v^{16} v3^5 - 1.676647904\,10^{30}\,v^{16} v3^9 \\
& - 1.888346556\,10^{29}\,v^{16} v3^{10} + 5.333963550\,10^9\,v^{16} v3^{11} + 6.23978001\,10^8\,v^{16} v3^{12} - 2.347307064\,10^{31}\,v^{10} v3^9 \\
& + 5.229555090\,10^{30}\,v^{10} v3^{10} - 3.709352560\,10^{20}\,v^{10} v3^{11} - 9.374186485\,10^{10}\,v^{10} v3^{12} + 9.142675110\,10^{31}\,v^{11} v3^9 \\
& + 2.090922903\,10^{22}\,v^{11} v3^{10} + 8.905757360\,10^{19}\,v^{11} v3^{11} - 3.617136838\,10^{10}\,v^{11} v3^{12} - 2.347307065\,10^{31}\,v^{12} v3^9 \\
& + 1.034347964\,10^{30}\,v^{12} v3^{10} - 2.967482048\,10^{20}\,v^{12} v3^{11} + 2.554614344\,10^{10}\,v^{12} v3^{12} + 5.079263950\,10^{31}\,v^{13} v3^9 \\
& + 5.405983040\,10^{21}\,v^{13} v3^{10} + 4.947643038\,10^{19}\,v^{13} v3^{11} + 1.361436500\,10^{10}\,v^{13} v3^{12} - 5.079263950\,10^{31}\,v^7 v3^9 \\
& + 3.875811498\,10^{22}\,v^7 v3^{10} - 4.947642948\,10^{19}\,v^7 v3^{11} - 1.244643334\,10^{11}\,v^7 v3^{12} + 7.853968510\,10^{30}\,v^8 v3^{10} \\
& - 1.940661756\,10^{11}\,v^8 v3^{12} + 5.079263950\,10^{31}\,v^9 v3^9 + 3.875811498\,10^{22}\,v^9 v3^{10} + 4.947642948\,10^{19}\,v^9 v3^{11} \\
& - 1.244643334\,10^{11}\,v^9 v3^{12} - 4.947643038\,10^{19}\,v^3 v3^{11} + 1.361436500\,10^{10}\,v^3 v3^{12} + 2.347307065\,10^{31}\,v^4 v3^9 \\
& + 1.034347964\,10^{30}\,v^4 v3^{10} + 2.967482048\,10^{20}\,v^4 v3^{11} + 2.554614344\,10^{10}\,v^4 v3^{12} - 9.142675110\,10^{31}\,v^5 v3^9 \\
& + 2.090922903\,10^{22}\,v^5 v3^{10} - 8.905757360\,10^{19}\,v^5 v3^{11} - 3.617136838\,10^{10}\,v^5 v3^{12} + 2.347307064\,10^{31}\,v^6 v3^9 \\
& + 5.229555090\,10^{30}\,v^6 v3^{10} + 3.709352560\,10^{20}\,v^6 v3^{11} - 9.374186485\,10^{10}\,v^6 v3^{12}
\end{aligned}
$$

(A.3)